JJEES

JJEES (2024) 15 (4): 307-316
ISSN 1995-6681

Jordan Journal of Earth and Environmental Sciences

Geoscientific Applications of Atomic Structure Calculations for Fe Ions (Fe II–Fe V) Using FAC Code

Safeia Hamasha* and Maher Abu-Alrous

Department of Physics, The Hashemite University, P.O. Box 330127, Zarqa 13133, Jordan

Received on October 14, 2024; Accepted on December 14, 2024

Abstract

This study presents atomic structure and spectral calculations for iron ions (Fe II–Fe V) using the Fully Relativistic Configuration Interaction (RCI) approach of the Flexible Atomic Code (FAC). The method generates critical atomic data, including energy levels, transition probabilities, wavelengths, oscillator strengths, and radiative rates, all of which are essential for geoscientific applications. It successfully identifies major spectral features across various transition bands, which are particularly significant for mineral spectroscopy under high-temperature and high-pressure conditions.

FAC's relativistic approach achieves remarkable accuracy in fine-structure details and wavelength precision, especially for higher ionization states, aligning closely with data from the National Institute of Standards and Technology (NIST). This precision makes it invaluable for applications requiring detailed spectroscopic data, such as studies of Deep-Earth mineral stability and high-resolution spectroscopic analyses. The calculated spectra span the extreme ultraviolet (EUV) to ultraviolet (UV) ranges, offering valuable insights into the behavior of iron ions within the Earth's crust and mantle, where extreme conditions drive mineral formation and transformation.

These findings provide essential atomic data for modeling iron-bearing minerals and support various applications, including mineral exploration, remote sensing, and geochemical modeling. The dual-method approach employed in this study balances computational efficiency with spectral accuracy, offering flexibility for future research. Expanding this methodology to include additional transition metals could enhance atomic datasets, broadening its relevance across geophysical and other scientific applications.

Keywords: *Iron ions, atomic structure, FAC code, mineral stability, geosciences, electronic configurations.*

1. Introduction

Iron is among the most abundant and influential elements in the Earth's crust, mantle, and core, playing a pivotal role in shaping planetary structure and driving both geophysical and geochemical processes. Its diverse oxidation states, ranging from neutral Fe I to highly ionized Fe ions, make it a central subject in studies of mineral stability and redox dynamics within geosciences (Khudhur et al., 2018; Tarawneh et al., 2021). Research has shown that iron significantly contributes to the Earth's magnetic field through its core interactions and influences phase transformations and mineral stability in silicate minerals in the crust and mantle (Zeng et al., 2008; Bovolo, 2005). Additionally, iron participates in redox reactions that regulate the cycling of major elements like oxygen and sulfur under high-temperature and high-pressure conditions (Frost & McCammon, 2008; O'Neill et al., 2018).

In geochemical studies, accurate atomic data for ionized iron is indispensable. Iron ions dominate the electronic structure of numerous minerals, influencing the spectral lines observed in mineral samples, particularly under varying environmental conditions in the Earth's crust and upper mantle (Badro et al., 2013; Abusalem et al., 2019). Investigations into the behavior of Fe ions under extreme pressure and temperature conditions have revealed that their spectral data provide valuable insights for applications in remote sensing, mineral exploration, and modeling Deep-Earth geochemistry (Li et al., 2020).

To generate precise atomic data, researchers employ tools such as the Cowan code and the Flexible Atomic Code (FAC). These computational methods enable highly accurate calculations of spectral lines, energy levels, and transition probabilities (Cowan, 1981; Gu, 2008). FAC, freely available through the International Atomic Energy Agency (https://www-amdis.iaea.org/FAC/), is particularly suited for studying complex electronic configurations in Fe ions.

Previous work by Sultana Nahar and colleagues utilized fully relativistic methods to calculate oscillator strengths, lifetimes, and fine-structure transitions across multiple ionization states of iron (Nahar, 2008; Nahar & Pradhan, 2011). Their benchmark data, particularly for highly ionized states, has been instrumental in astrophysical and plasma studies. Nahar's work demonstrated high precision in line positions and transition probabilities, particularly for forbidden transitions critical to modeling low-density environments.

* Corresponding author e-mail: safeia@hu.edu.jo

Building on this foundation, the present study employs FAC's Fully Relativistic Configuration Interaction (RCI) method to assess computational efficiency and spectral accuracy in geoscientific applications. This approach is essential for accurately modeling Fe ions, particularly in high-ionization states like Fe IV and Fe V, where electronic complexity requires advanced methods to account for relativistic and electron-correlation effects (Gu, 2008).

This paper presents the results of atomic structure and spectral calculations for Fe II–Fe V ions, alongside synthetic spectra and identified strong transition lines. These prominent transitions are expected to appear in observed or experimental spectra of Fe ions. The findings are highly relevant for high-precision modeling of iron-bearing minerals, which is increasingly important for geophysical and environmental studies.

2. Theoretical Background: Fully Relativistic Configuration Interaction (RCI) Method

To construct a comprehensive atomic database for iron ions (Fe II to Fe V), the Fully Relativistic Configuration Interaction (RCI) method of the Flexible Atomic Code (FAC) is employed. This method provides detailed insights into the atomic structure and spectral properties of atoms and ions. By utilizing the Dirac equation, the FAC-RCI method incorporates relativistic effects, which are critical for accurately modeling complex multi-electron systems such as iron and its ions.

This approach enables the precise calculation of key spectral properties, including energy levels, transition wavelengths, and radiative probabilities, facilitating a robust analysis of the atomic structure of iron ions under relativistic constraints (Gu, 2008). Such precision is crucial for applications that require detailed spectroscopic data, especially in high-energy geophysical and geochemical contexts.

For a more in-depth understanding of relativistic atomic structure and configuration interaction, readers are encouraged to consult the foundational work of Grant (2007) and the comprehensive discussions on many-body relativistic treatments in atomic physics by Lindgren and Morrison (2012). These resources provide valuable context for the theoretical framework underpinning the FAC-RCI method.

3. Results and Discussion

The Flexible Atomic Code (FAC) was employed to calculate atomic structure data for Fe II, Fe III, Fe IV, and Fe V ions, with a focus on the Fully Relativistic Configuration Interaction (RCI) method. This approach accounts for electron-electron correlation effects and spin-orbit coupling, both of which are crucial for accurately modeling complex multi-electron systems like iron ions. FAC generates detailed atomic data, including transition energies, optically allowed transition rates, oscillator strengths, and radiative probabilities for each ionized state.

The calculations primarily involved transitions of M-shell electrons (n = 3) to higher energy levels (n = 4, 5, 6, 7, and 8). These transitions span the extreme ultraviolet (EUV) and ultraviolet (UV) spectral ranges, making them particularly relevant for modeling the behavior of iron ions under the high-temperature and high-pressure conditions often encountered in geophysical and geological contexts. FAC's relativistic framework is especially advantageous for capturing fine-structure splitting in highly ionized states, where relativistic effects significantly impact atomic structure calculations.

The study focused on four ionization states of iron: Mn-like Fe (Fe II), Cr-like Fe (Fe III), V-like Fe (Fe IV), and Ti-like Fe (Fe V) ions. FAC computations were used to determine electron transitions from the M-shell (n = 3) to higher shells, producing essential atomic parameters such as energy levels, transition probabilities, and oscillator strengths. Synthetic spectra for these ions were generated using Doppler line broadening profiles at a temperature T_{Dopp}=1200 ºK, sufficient to produce clear and well-defined spectral lines. Figures 1–4 illustrate these synthetic spectra, covering the spectral ranges of interest for each ion.

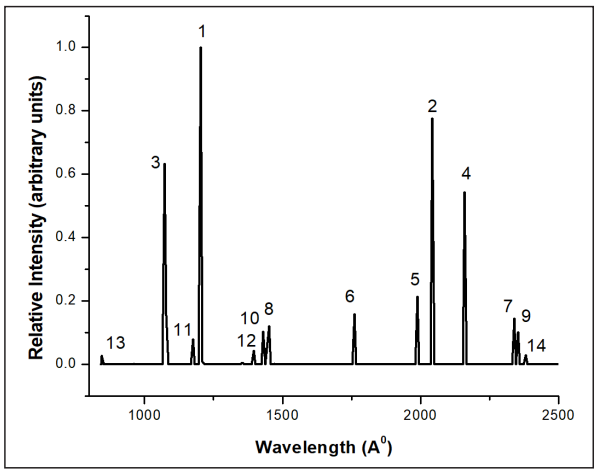

Figure 1. Synthetic spectrum of Fe II ion produced by FAC's RCI method, indicating strong transitions within the UV spectral region.

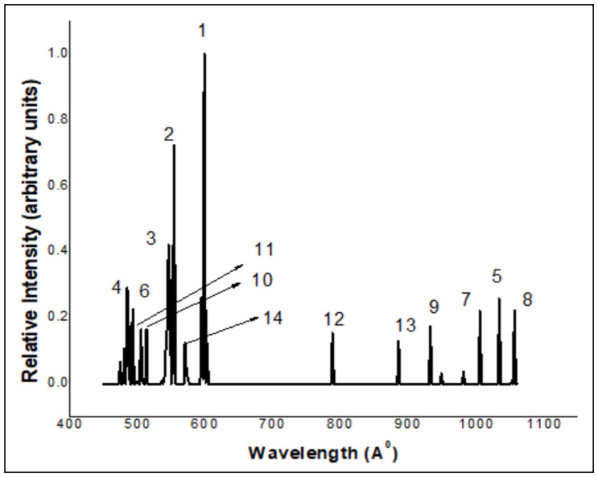

Figure 2. Synthetic spectrum of Fe III ion produced by FAC's RCI method, indicating strong transitions within the EUV to UV spectral region.

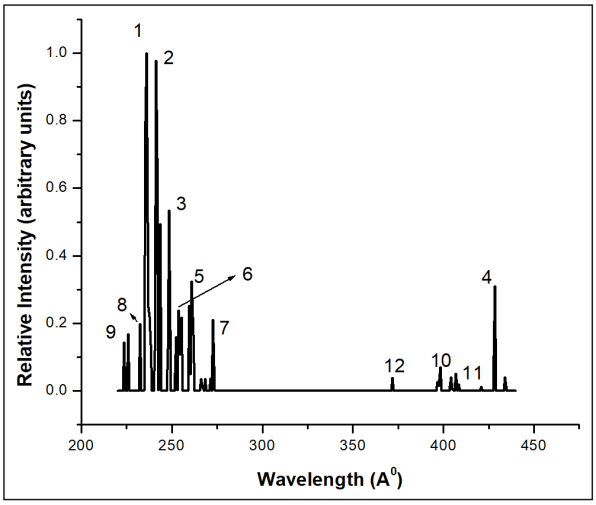

Figure 3. Synthetic spectrum of Fe IV ion produced by FAC's RCI method, indicating strong transitions within the EUV spectral region.

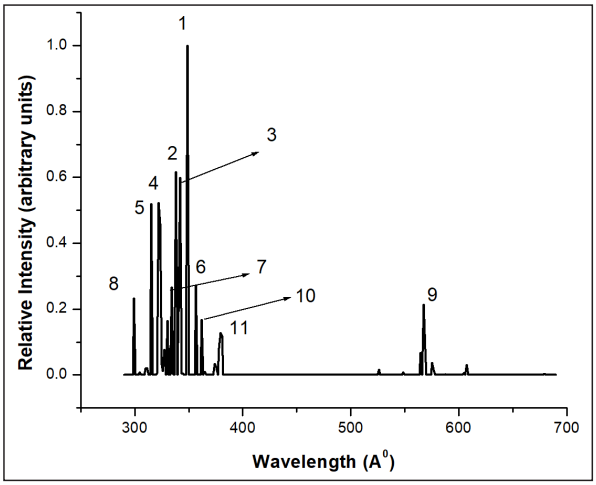

Figure 4. Synthetic spectrum of Fe V ion produced by FAC's RCI method, indicating strong transitions within the EUV spectral region.

The ground-state configurations and significant transitions for each ion are detailed in Table 1. These configurations form the basis for spectral analysis, with transitions grouped according to their intensity and spectral significance. The most important spectral lines expected to appear in experimental spectra are identified and labeled in the synthetic spectra. These prominent lines, predominantly 3-4 transitions, are summarized in Table 2. Table 2 presents the peak number (peak #), the electronic configuration of the upper state (configuration (up)), the parity P of the upper state (P (up)), the total angular momentum of the upper state (J (up)), the electronic configuration of the lower state (configuration (low)), the parity P of the lower state (P (low)), the total angular momentum of the lower state (J (low)), the transition energy in electron volts (ΔE), the weighted oscillator strength (gf_{ij}), the radiative transition probability (A_r (s^{-1})), the calculated wavelength in angstroms (λ(Å)) and the wavelength listed in NIST database in angstroms (λ_{NIST} (Å)).

Transitions from 3-5 and 3-6 groups, while present, are less intense and exhibit shorter wavelengths. Transitions from 3-6 are particularly weak and unlikely to appear in experimental spectra under standard conditions. When compared with the NIST database, all calculated lines in this study were found to be consistent with listed transitions. However, this work focuses specifically on strong transitions that are most likely to appear in real iron spectra under geophysical conditions, emphasizing their relevance for applications such as mineral spectroscopy and geochemical modeling. Detailed findings of each ion are offered in the following subsections:

3.1 Mn-like Fe (Fe II) ion strong transitions

The ground-state configuration of Fe II was identified as [Ne] $3s^2\ 3p^6\ 4s^2\ 3d^5$ or equivalently [Ar] $4s^2\ 3d^5$. To streamline the analysis, only single-electron excitations were considered, and transitions with low radiative probabilities were omitted, as these are unlikely to appear in observed Fe ion spectra. This selection resulted in a large set of significant transitions, among which the strongest lines predominantly occurred within the 3d–4f transition group. The most intense line was observed at a wavelength of λ = 1201 Å.

The full spectral range for Fe II transitions spans from 900 Å to 2500 Å, placing these transitions within the ultraviolet (UV) spectrum, a region critical for high-energy geophysical applications. While Fe II exhibits a rich array of transition lines, this study focused on the strongest bands likely to appear under normal conditions in experimental spectra. Table 2 summarizes the most prominent transitions, while Figure 1 presents the synthetic spectrum generated for Fe II using a Doppler line profile at a broadening temperature T_{Dopp}=1200ºK. This temperature highlights the notable contributions of 3d–4f and 3d–4p transitions.

Higher-order transitions, such as 3d–5p and 3d–6p, were also identified in the spectra but exhibit significantly lower intensities compared to the dominant 3d–4 transitions. These weaker lines are less likely to have a notable presence in real Fe II spectra under typical geophysical conditions.

The calculated spectra for Fe II reveal distinct intensity distributions, which are valuable for developing geophysical models. Accurate representation of UV emissions is essential for studying high-temperature mineral phases and the behavior of iron ions in Earth's crust and mantle. By identifying strong transitions and high-probability configurations, this data enables more precise modeling of iron-bearing minerals under extreme conditions, contributing to the understanding of high-temperature and high-pressure geochemical processes.

3. 2 Cr-like Fe (Fe III) ion strong transitions

for Fe III, the electronic configurations and prominent transition lines are detailed in Tables 1 and 2. Similar to Fe II, the transitions primarily involve M-shell electrons (n = 3) moving to outer shells (n = 4, 5, 6, 7, and 8). The ground-state configuration, [Ne] $3s^2\ 3p^6\ 3d^6$, forms the foundation for transition calculations. Single-electron excitations were considered, and transitions with significant probabilities were filtered, resulting in over 357 prominent transitions, summarized in Table 2. Among these, the strongest transition occurs within the 3d–4f series at a wavelength of λ = 599 Å.

The full spectral range for allowed transitions in Fe III

spans 370 Å to 1075 Å, positioning these lines within the Extreme Ultraviolet (EUV) to ultraviolet (UV) region. This range is critical for high-temperature applications in geosciences, including mineral stability modeling and phase transition studies. Figure 2 presents the synthetic spectrum generated using the FAC-RCI method, incorporating Doppler line broadening at a temperature T_{Dopp}=1200ºK. The spectrum highlights the dominance of 3d–4f transitions, specifically from [Ar] $4s^2\,3d^4$ to [Ar] $4s^2\,3d^3\,4f$. These transitions are followed in intensity by 3d–4p and then 3d–4s transitions.

The pronounced dominance of the 3d–4f transitions underscores a characteristic pattern in Fe III, where higher-energy excitations to f orbital produce intense spectral lines. This behavior is particularly valuable for applications requiring precise EUV data, such as studies of high-energy geochemical environments.

The FAC-derived spectra for Fe III provide a comprehensive dataset that captures fine-structure splitting and delivers precision in energy level spacing. These results align closely with the NIST database benchmarks, confirming the reliability of FAC for generating accurate atomic data. This level of detail is crucial for modeling the behavior of Fe III in high-energy geochemical contexts, such as those found in the Earth's upper mantle or during high-temperature mineral reactions. FAC's ability to accurately capture these transitions establishes its utility in studies of iron-bearing minerals, where such detailed spectral data are indispensable.

3.3 V-like Fe (Fe IV) ion strong transitions

The configurations and transition lines for Fe IV are depicted in Tables 1 and 2. They illustrate M-shell excitations from n = 3 to n = 4, 5, 6, 7, and 8 shells. The ground-state configuration of Fe IV ion is: [Ne] $3s^2\,3p^6\,4s^2\,3d^3$. The calculated spectral data for V-like Fe ion is done by considering single electron excitations, where the calculated data contains both strong and weak transitions; therefore we filtered the data for strong transitions, resulting in 246 significant transitions. Two particularly strong transitions groups are identified; 3d-4f and 3d-4p groups. The strongest transition is identified to be from [Ar] $3d_{3/2}^{\ 2}\,3d_{5/2}^{\ 2}\,4f_{5/2}$ (J_f) to [Ar] $3d_{3/2}^{\ 2}\,3d_{5/2}^{\ 3}$ (J_i) with λ = 348 Å. The synthetic spectrum of Fe IV ion is shown in Figure 3, presenting dominant 3d–4d transitions, and the spectral range is in the EUV range, which are of particular significance for geochemical analysis.

Among 3-5 transitions, the strongest calculated transition was in the 3d–5f series, with a wavelength of λ = 223.04 Å, but because of 3-5 transitions have low radiative transition probabilities they might not appear in real experimental Fe IV ion's spectrum. The entire spectral range of Fe IV ion for optically allowed transitions spans from 190 Å to 435 Å, placing these transitions within the Extreme Ultraviolet (EUV) region. This range is particularly relevant for applications in high-temperature geophysical environments where EUV data is critical.

The FAC-calculated data for Fe IV ion's 3d–4f and 3d–4p transitions provide high-resolution insight into fine-structure splitting and transition probabilities, line up closely with experimental and NIST database. These transitions, which produce strong emission lines within the EUV range, are highly relevant for geochemical and mineralogical studies, as they enable detailed modeling of Fe IV ion's behavior under extreme conditions, such as high pressures and temperatures in Earth's upper mantle. FAC's precise handling of these transitions in Fe IV ion underscores its value in generating accurate atomic data, which is crucial for simulating the spectroscopic properties of iron-bearing minerals. This level of detail enhances our understanding of the spectroscopic behavior of Fe IV in geological environments and supports its application in remote sensing and high-temperature mineral phase studies.

3. 4 Ti-like Fe (Fe V) ion strong transitions

For Fe V ion, the electronic configurations and strongest transitions are provided in Tables 1 and 2. Calculated spectral data presents M-shell transitions from n = 3 to outer shells (n = 4, 5, 6, 7, and 8). The ground-state configuration for Fe V ion is: [Ne] $3s^2\,3p^6\,4s^2\,3d^2$, which serves as the reference point for this ion's spectroscopic calculations. Like prior ions, only single-electron excitations were considered. The produced spectral data table contains large file of strong and weak transitions, so it was filtered to strong transition lines only. This filtering process resulted in 300 significant transitions. Transitions that contribute to the Fe V spectrum are summarized in Table 2. Among the identified transitions, the most prominent line is in the 3d–4f series, with a wavelength of λ = 236 Å. This intense transition, a characteristic of Fe V ion, represents the highest transition rate observed across the Fe V ion series, signifying strong radiative decay in this particular configuration. The spectroscopic data for Fe V ion, particularly the intense 3d–4f transitions, is crucial for understanding iron's behavior in geoscientific contexts where high ionization states are present within high-temperature mineral phases or under extreme conditions in the Earth's mantle. These findings underscore Fe V ion's relevance in studies of mineral stability and transformation, as well as in modeling the spectroscopic properties of iron-bearing minerals in geological environments.

The complete spectral range for allowed transitions in Fe V ion spans the spectral range from 223 Å to 434 Å, situating these transitions firmly within the extreme ultraviolet (EUV) region, which is pertinent to high-energy geophysical environments. The synthetic spectrum for Fe V ion is displayed in Figure 4. Doppler line profile is used to account for temperature-based broadening.

This EUV spectral profile is particularly relevant for high-temperature geoscience applications, as it provides insight into the behavior of iron ions under extreme conditions, such as those found in the Earth's upper mantle or core-mantle boundary, where temperatures exceed several thousand Kelvin. In these environments, iron undergoes high degrees of ionization, and its EUV emissions can be critical for remote sensing in high-energy astrophysical and geophysical contexts. Additionally, Fe ions prominent 3d–nf transitions contribute significantly to the opacity of iron in high-temperature and high-pressure mineral phases,

influencing the thermal conductivity and stability of iron-bearing compounds within Earth's mantle. This data can support simulations of mantle convection, mineral phase transitions, and core-mantle boundary dynamics, enhancing our understanding of Earth's internal processes and the thermal evolution of planetary interiors where iron plays a key role.

FAC-RCI method is used to produce synthetic spectra for Fe II–Fe V with strong alignment in major spectral features, which are critical for mineral spectroscopy in geosciences. This alignment in major transition lines is consistent with findings by Nahar (2008), where their results are listed in NIST database. Their work demonstrated similar patterns across Fe ionization states. Our results support the reliability of FAC- RCI methods in capturing key transitions for iron ions, providing confidence in their applicability across varied research fields. However, FAC's fully relativistic configuration interaction approach offers greater precision in resolving fine structures, especially for higher ionization states like Fe IV and Fe V. Nahar's work underscores the significance of fine structure in modeling highly ionized iron in low-density environments, such as those encountered in astrophysics. FAC's detailed fine-structure resolution is beneficial for geophysical models requiring accuracy in high-ionization states.

FAC's findings are aligned closely with NIST database and compares well with the precision achieved in Nahar's results for highly ionized Fe ions used in astrophysical spectra. This precision is valuable for applications that require exact wavelength data, such as high-resolution mineral spectroscopy.

4. Summary and Conclusions

This study demonstrated the effectiveness of FAC's Fully Relativistic Configuration Interaction (RCI) method in calculating atomic data for Fe II–Fe V ions. The results align closely with NIST data, though FAC exhibited high accuracy in fine-structure details and wavelength precision, particularly for high ionization states. These findings underscore FAC's potential for high-precision mineral spectroscopy and Deep-Earth geophysics, where accurate fine-structure and relativistic corrections are critical.

Conflict of Interest

The authors declare that they have no conflicts of interest.

References

Abusalem, M, Awwad, A., Ayad, J., Abu Rayyan, A. (2019). Green Synthesis of Hematite (A-Fe2O3) Nanoparticles Using Extract Influenced Seed Germination and Seedling Growth of Tomatos. Jordan Journal of Earth and Environmental Sciences, 10(3), 161-166.

Badro, J., Fiquet, G., François, Guyot, F., Rueff, J. P., Struzhkin, V. V., Vankó, G., Monaco, G. (2003). Iron Partitioning in Earth's Mantle: Toward a Deep Lower Mantle Discontinuity. Science: 789-791. doi:10.1126/science.1081311. https://www.science.org/doi/abs/10.1126/science.1081311

Bovolo, C. I. (2005). The physical and chemical composition of the lower mantle. Philosophical Transactions A, 363(1837):2811-35. Doi: 10.1098/rsta.2005.1675

Cowan, R.D. (1981) The Theory of Atomic Structure and Spectra. University of California Press, Berkeley.

Frost, D. J., & McCammon, C. A. (2008). The redox state of Earth's mantle. Annual Review of Earth and Planetary Sciences, 36(1):389-420. Doi: 10.1146/annurev.earth.36.031207.124322

https://doi.org/10.1146/annurev.earth.36.031207.124322

Grant, I. P. (2007). Relativistic quantum theory of atoms and molecules: Theory and computation. Springer. Doi: https://doi.org/10.1007/978-0-387-35069-1

Gu, M. F. (2008). Flexible Atomic Code. Canadian Journal of Physics, 86: 675-689.

https://doi.org/10.1139/p07-197

Khudhur, N. S., Shelan Mustafa Khudhur, S.M., Ahmad, I. N. (2018). An Assessment of Heavy Metal Soil Contamination in a Steel Factory and the Surrounding Area in Erbil City. JJEES 9(1),1-11.

Li, X., Liu, J., Hu, Q., Li, J., & Mao, Z. (2020). Iron oxides in Earth's lower mantle. Journal of Geophysical Research: Solid Earth, 125(11), e2020JB020706. doi:10.1029/2020JB020706.

Lindgren, I., & Morrison, J. (2012). Atomic many-body theory (2nd ed.). Barnes & Noble, Springer.

Nahar, S. N. (2008). Relativistic atomic data for Fe ions: Energy levels and transition probabilities for Fe XVII–Fe XXV. Physical Review A, 78(5), 052501. doi:10.1103/PhysRevA.78.052501

Nahar, S. N., & Pradhan, A. K. (2011). High-precision calculations for Fe XVII–Fe XXVI: Oscillator strengths and lifetimes. The Astrophysical Journal Supplement Series, 194(2), 43. doi:10.1088/0067-0049/194/2/43

National Institute of Standards and Technology (NIST). (n.d.). Atomic Spectra Database. Retrieved from https://www.nist.gov/pml/atomic-spectra-database.

O'Neill, H. S. C., Berry, A. J., Guilherme Mallmann, G. (2018). The oxidation state of iron in Mid-Ocean Ridge Basaltic (MORB) glasses: Implications for their petrogenesis and oxygen fugacities. Earth and Planetary Science Letters, 504:152-162. https://doi.org/10.1016/j.epsl.2018.10.002

Tarawneh, K., Eleyan, I., Alalwan, R., Sallam,S, Hammad,S. (2021) Assessment of heavy metals contamination levels in surfaces soil in Baqa'a area, Jordan. JJEES 12(4): 285-294 ISSN

Zeng, Z. Y., Hu, C. E., Chen, X. R., and Ling-Cang Cai, L. C., Jing, F. Q. (2008). Magnetism and phase transitions of iron under pressure. Journal of Physics: Condensed Matter, 20(42): 425217. Doi:10.1088/0953-8984/20/42/425217. https://dx.doi.org/10.1088/0953-8984/20/42/425217.

Table 1. Electronic configurations that were used in FAC-RCI code for transitions from n= 4 → 5, 6, 7, 8 transitions in Fe ions (Fe II–Fe V).

Ion	Shell number	Electron Configuration
Fe II	n=4	Ground State: $1s^2\ 2s^2\ 2p^6\ 3s^2\ 3p^6\ 3d^6\ 4s^1$ or $[Ar^{18}]\ 3d^6\ 4s^1$ $[Ar^{18}]\ 3d^6\ 4p^1$, $[Ar^{18}]\ 3d^6\ 4d^1$, $[Ar^{18}]\ 3d^6\ 4p^1 4f^1$
	n= 5	$[Ar^{18}]\ 3d^6\ 5s^1$, $[Ar^{18}]\ 3d^6\ 5p^1$, $[Ar^{18}]\ 3d^6\ 5d^1$, $[Ar^{18}]\ 3d^6\ 5f^1$, $[Ar^{18}]\ 3d^6\ 5g^1$
	n= 6	$[Ar^{18}]\ 3d^6\ 6s^1$, $[Ar^{18}]\ 3d^6\ 6p^1$, $[Ar^{18}]\ 3d^6\ 6d^1$, $[Ar^{18}]\ 3d^6\ 6f^1$, $[Ar^{18}]\ 3d^6\ 6g^1$, $[Ar^{18}]\ 3d^6\ 6h^1$
	n= 7	$[Ar^{18}]\ 3d^6\ 7s^1$, $[Ar^{18}]\ 3d^6\ 7p^1$, $[Ar^{18}]\ 3d^6\ 7d^1$, $[Ar^{18}]\ 3d^6\ 7f^1$, $[Ar^{18}]\ 3d^6\ 7g^1$, $[Ar^{18}]\ 3d^6\ 7h^1$
	n= 8	$[Ar^{18}]\ 3d^6\ 8s^1$, $[Ar^{18}]\ 3d^6\ 8p^1$, $[Ar^{18}]\ 3d^6\ 8d^1$, $[Ar^{18}]\ 3d^6\ 8f^1$, $[Ar^{18}]\ 3d^6\ 8g^1$, $[Ar^{18}]\ 3d^6\ 8h^1$
Fe III	n= 4	Ground State: $1s^2\ 2s^2\ 2p^6\ 3s^2\ 3p^6\ 3d^6\ 4s^2$ or $[Ar^{18}]\ 3d^6\ 4s^2$ $[Ar^{18}]\ 3d^6\ 4s^1\ 4p^1$, $[Ar^{18}]\ 3d^6\ 4s^1 4d^1$, $[Ar^{18}]\ 3d^6\ 4s^1\ 4f^1$
	n=5	$[Ar^{18}]\ 3d^6\ 4s^1\ 5p^1$, $[Ar^{18}]\ 3d^6\ 4s^1 5d^1$, $[Ar^{18}]\ 3d^6\ 4s^1\ 5f^1$, $[Ar^{18}]\ 3d^6\ 4s^1\ 5g^1$,
	n= 6	$[Ar^{18}]\ 3d^6\ 4s^1\ 6p^1$, $[Ar^{18}]\ 3d^6\ 4s^1$ 6d1, $[Ar^{18}]\ 3d^6\ 4s^1\ 6f^1$, $[Ar^{18}]\ 3d^6\ 4s^1\ 6g^1$, $[Ar^{18}]\ 3d^6\ 4s^1\ 6h^1$
	n= 7	$[Ar^{18}]\ 3d^6\ 4s^1\ 7p^1$, $[Ar^{18}]\ 3d^6\ 4s^1$ 7d1, $[Ar^{18}]\ 3d^6\ 4s^1\ 7f^1$, $[Ar^{18}]\ 3d^6\ 4s^1\ 7g^1$, $[Ar^{18}]\ 3d^6\ 4s^1\ 7h^1$
	n= 8	$[Ar^{18}]\ 3d^6\ 4s^1\ 8p^1$, $[Ar^{18}]\ 3d^6\ 4s^1$ 8d1, $[Ar^{18}]\ 3d^6\ 4s^1\ 8f^1$, $[Ar^{18}]\ 3d^6\ 4s^1\ 8g^1$, $[Ar^{18}]\ 3d^6\ 4s^1\ 8h^1$
Fe IV	n= 4	Ground State: $1s^2\ 2s^2\ 2p^6\ 3s^2\ 3p^6\ 3d^6\ 4s^2\ 4p^1$ or $[Ar^{18}]\ 3d^6\ 4s^2\ 4p^1$ $[Ar^{18}]\ 3d^6\ 4s^1\ 4p^2$, $[Ar^{18}]\ 3d^6\ 4s^2 4d^1$, $[Ar^{18}]\ 3d^6\ 4s^2\ 4f^1$, $[Ar^{18}]\ 3d^6\ 4s^1\ 4d^2$,$[Ar^{18}]\ 3d^6\ 4s^1\ 4f^2$
	n=5	$[Ar^{18}]\ 3d^6\ 4s^2\ 5p^1$, $[Ar^{18}]\ 3d^6\ 4s^2 5d^1$, $[Ar^{18}]\ 3d^6\ 4s^2\ 5f^1$, $[Ar^{18}]\ 3d^6\ 4s^2\ 5g^1$, $[Ar^{18}]\ 3d^6\ 4s^1\ 5p^2$, $[Ar^{18}]\ 3d^6\ 4s^1 5d^2$, $[Ar^{18}]\ 3d^6\ 4s^2\ 5f^1$, $[Ar^{18}]\ 3d^6\ 4s^2\ 5g^1$
	n= 6	$[Ar^{18}]\ 3d^6\ 4s^2\ 6p^1$, $[Ar^{18}]\ 3d^6\ 4s^2$ 6d1, $[Ar^{18}]\ 3d^6\ 4s^2\ 6f^1$, $[Ar^{18}]\ 3d^6\ 4s^1\ 6g^1$, $[Ar^{18}]\ 3d^6\ 4s^2\ 6h^1$, $[Ar^{18}]\ 3d^6\ 4s^1\ 6p^2$, $[Ar^{18}]\ 3d^6\ 4s^1\ 6d^2$, $[Ar^{18}]\ 3d^6\ 4s^1\ 6f^2$, $[Ar^{18}]\ 3d^6\ 4s^1\ 6g^2$, $[Ar^{18}]\ 3d^6\ 4s^1\ 6h^2$
	n= 7	$[Ar^{18}]\ 3d^6\ 4s^2\ 7p^1$, $[Ar^{18}]\ 3d^6\ 4s^2$ 7d1, $[Ar^{18}]\ 3d^6\ 4s^2\ 7f^1$, $[Ar^{18}]\ 3d^6\ 4s^2\ 7g^1$, $[Ar^{18}]\ 3d^6\ 4s^2\ 7h^1$, $[Ar^{18}]\ 3d^6\ 4s^1\ 7p^2$, $[Ar^{18}]\ 3d^6\ 4s^1\ 7d^2$, $[Ar^{18}]\ 3d^6\ 4s^1\ 7f^2$, $[Ar^{18}]\ 3d^6\ 4s^2\ 7g^1$, $[Ar^{18}]\ 3d^6\ 4s^1\ 7h^2$
	n= 8	$[Ar^{18}]\ 3d^6\ 4s^2\ 78p^1$, $[Ar^{18}]\ 3d^6\ 4s^2$ 8d1, $[Ar^{18}]\ 3d^6\ 4s^2\ 8f^1$, $[Ar^{18}]\ 3d^6\ 4s^2\ 8g^1$, $[Ar^{18}]\ 3d^6\ 4s^2\ 8h^1$, $[Ar^{18}]\ 3d^6\ 4s^1\ 8p^2$, $[Ar^{18}]\ 3d^6\ 4s^1\ 8d^2$, $[Ar^{18}]\ 3d^6\ 4s^1\ 8f^2$, $[Ar^{18}]\ 3d^6\ 4s^2\ 8g^1$, $[Ar^{18}]\ 3d^6\ 4s^1\ 8h^2$
Fe V	n= 4	Ground State: $1s^2\ 2s^2\ 2p^6\ 3s^2\ 3p^6\ 3d^6\ 4s^2\ 4p^2$ or $[Ar^{18}]\ 3d^6\ 4s^2\ 4p^2$ $[Ar^{18}]\ 3d^6\ 4s^2\ 4p^1\ 4d^1$, $[Ar^{18}]\ 3d^6\ 4s^2\ 4p^1\ 4f^1$, $[Ar^{18}]\ 3d^6\ 4s^2\ 4d^1\ 4f^1$, $[Ar^{18}]\ 3d^6\ 4s^1\ 4p^2\ 4d^1$, $[Ar^{18}]\ 3d^6\ 4s^1\ 4f^3$, $[Ar^{18}]\ 3d^6\ 4s^1\ 4p^2\ 4f^1$, $[Ar^{18}]\ 3d^6\ 4s^1\ 4p^1\ 4f^2$, $[Ar^{18}]\ 3d^6\ 4s^1\ 4p^3$, $[Ar^{18}]\ 3d^6\ 4s^1\ 4d^3$ $[Ar^{18}]\ 3d^6\ 4s^1\ 4f^4$
	n=5	$[Ar^{18}]\ 3d^6\ 4s^2\ 4p^1\ 5d^1$, $[Ar^{18}]\ 3d^6\ 4s^2\ 4p^1\ 5f^1$, $[Ar^{18}]\ 3d^6\ 4s^2\ 4d^1\ 5f^1$, $[Ar^{18}]\ 3d^6\ 4s^1\ 4p^2\ 5d^1$, $[Ar^{18}]\ 3d^6\ 4s^1\ 5f^3$, $[Ar^{18}]\ 3d^6\ 4s^1\ 4p^2\ 5f^1$, $[Ar^{18}]\ 3d^6\ 4s^1\ 4p^1\ 5f^2$, $[Ar^{18}]\ 3d^6\ 4s^1\ 5p^3$, $[Ar^{18}]\ 3d^6\ 4s^1\ 5d^3$ $[Ar^{18}]\ 3d^6\ 4s^1\ 5f^4$
	n= 6	$[Ar^{18}]\ 3d^6\ 4s^2\ 4p^1\ 6d^1$, $[Ar^{18}]\ 3d^6\ 4s^2\ 4p^1\ 6f^1$, $[Ar^{18}]\ 3d^6\ 4s^2\ 4d^1\ 6f^1$, $[Ar^{18}]\ 3d^6\ 4s^1\ 4p^2\ 6d^1$, $[Ar^{18}]\ 3d^6\ 4s^1\ 6f^3$, $[Ar^{18}]\ 3d^6\ 4s^1\ 4p^2\ 6f^1$, $[Ar^{18}]\ 3d^6\ 4s^1\ 4p^1\ 6f^2$, $[Ar^{18}]\ 3d^6\ 4s^1\ 6p^3$, $[Ar^{18}]\ 3d^6\ 4s^1\ 6d^3$ $[Ar^{18}]\ 3d^6\ 4s^1\ 6f^4$
	n= 7	$[Ar^{18}]\ 3d^6\ 4s^2\ 4p^1\ 7d^1$, $[Ar^{18}]\ 3d^6\ 4s^2\ 4p^1\ 7f^1$, $[Ar^{18}]\ 3d^6\ 4s^2\ 4d^1\ 7f^1$, $[Ar^{18}]\ 3d^6\ 4s^1\ 4p^2\ 7d^1$, $[Ar^{18}]\ 3d^6\ 4s^1\ 7f^3$, $[Ar^{18}]\ 3d^6\ 4s^1\ 4p^2\ 7f^1$, $[Ar^{18}]\ 3d^6\ 4s^1\ 4p^1\ 7f^2$, $[Ar^{18}]\ 3d^6\ 4s^1\ 7p^3$, $[Ar^{18}]\ 3d^6\ 4s^1\ 7d^3$ $[Ar^{18}]\ 3d^6\ 4s^1\ 7f^4$
	n= 8	$[Ar^{18}]\ 3d^6\ 4s^2\ 4p^1\ 8d^1$, $[Ar^{18}]\ 3d^6\ 4s^2\ 4p^1\ 8f^1$, $[Ar^{18}]\ 3d^6\ 4s^2\ 4d^1\ 8f^1$, $[Ar^{18}]\ 3d^6\ 4s^1\ 4p^2\ 8d^1$, $[Ar^{18}]\ 3d^6\ 4s^1\ 8f^3$, $[Ar^{18}]\ 3d^6\ 4s^1\ 4p^2\ 8f^1$, $[Ar^{18}]\ 3d^6\ 4s^1\ 4p^1\ 8f^2$, $[Ar^{18}]\ 3d^6\ 4s^1\ 8p^3$, $[Ar^{18}]\ 3d^6\ 4s^1\ 8d^3$ $[Ar^{18}]\ 3d^6\ 4s^1\ 8f^4$

Table 2. Strong electric dipole transitions atomic data calculated for n=3- 4 of the iron ions Fe II–Fe V

peak #	configuration (up)	P (up)	J (up)	configuration (low)	P (low)	J (low)	ΔE (eV)	gfij	Ar (s^{-1})	λ (Å)	λ_{NIST}(Å)
Fe II											
1	$3d_{3/2}^2\ 3d_{5/2}^4\ 4f_{5/2}$	1	6.5	$3d_{3/2}^3\ 3d_{5/2}^4$	0	5.5	10.314	0.527	1.74E+08	1202.06	1203.84
1	$3d_{3/2}^2\ 3d_{5/2}^4\ 4f_{5/2}$	1	5.5	$3d_{3/2}^3\ 3d_{5/2}^4$	0	5.5	10.317	0.617	2.37E+08	1201.68	1201.55
1	$3d_{3/2}^2\ 3d_{5/2}^4\ 4f_{7/2}$	1	3.5	$3d_{3/2}^2\ 3d_{5/2}^5$	0	2.5	10.324	0.533	3.08E+08	1200.89	1200.89
2	$3d_{3/2}\ 3d_{5/2}^5\ ^4p_{1/2}$	1	3.5	$3d_{3/2}^3\ 3d_{5/2}^4$	0	3.5	5.082	0.723	1.01E+08	2439.54	--
2	$3d_{3/2}^3\ 3d_{5/2}^3\ 4p_{1/2}$	1	3.5	$3d_{5/2}^3$	0	4.5	6.070	0.733	1.47E+08	2042.55	--
3	$3d_{3/2}^2\ 3d_{5/2}^4\ 4f_{5/2}$	1	4.5	$3d_{3/2}^3\ 3d_{5/2}^4$	0	5.5	11.565	0.325	1.89E+08	1072.06	1071.58
3	$3d_{3/2}^2\ 3d_{5/2}^4\ 4f_{7/2}$	1	5.5	$3d_{3/2}^3\ 3d_{5/2}^4$	0	5.5	11.574	0.456	2.21E+08	1071.19	1071.25
3	$3d_{3/2}^2\ 3d_{5/2}^4\ 4f_{5/2}$	1	6.5	$3d_{3/2}^3\ 3d_{5/2}^4$	0	5.5	11.579	0.224	9.32E+07	1070.70	1070.12
4	$3d_{3/2}^2\ 3d_{5/2}^4\ 4p_{1/2}$	1	0.5	$3d_{5/2}^3$	0	1.5	5.741	0.257	1.84E+08	2159.72	--
4	$3d_{3/2}\ 3d_{5/2}^5\ ^4p_{1/2}$	1	1.5	$3d_{3/2}^3\ 3d_{5/2}^4$	0	2.5	5.740	0.392	1.40E+08	2160.06	--
5	$3d_{3/2}^2\ 3d_{5/2}^4\ ^4p_{1/2}$	1	4.5	$3d_{5/2}^3$	0	4.5	6.236	0.907	1.53E+08	1988.18	1988.66
5	$3d_{3/2}\ 3d_{5/2}^5\ ^4p_{1/2}$	1	3.5	$3d_{3/2}^3\ 3d_{5/2}^4$	0	3.5	6.224	0.536	1.13E+08	1991.93	1991.54
6	$3d_{3/2}^2\ 3d_{5/2}^4\ 4p_{1/2}$	1	1.5	$3d_{3/2}^2\ 3d_{5/2}^5$	0	2.5	7.041	0.281	1.51E+08	1760.84	1761.37
7	$3d_{3/2}^3\ 3d_{5/2}^3\ 4p_{1/2}$	1	1.5	$3d_{3/2}^3\ 3d_{5/2}^4$	0	2.5	5.300	0.308	9.38E+07	2339.13	--
8	$3d_{3/2}^3\ 3d_{5/2}^3\ 4f_{7/2}$	1	0.5	$3d_{3/2}^3\ 3d_{5/2}^4$	0	1.5	8.535	0.136	2.15E+08	1452.62	1452.40
8	$3d_{3/2}^3\ 3d_{5/2}^3\ 4f_{7/2}$	1	0.5	$3d_{3/2}^3\ 3d_{5/2}^4$	0	0.5	8.545	0.087	1.38E+08	1450.87	1450.86
9	$4p_{1/2}$	1	0.5	$3d_{3/2}^2\ 3d_{5/2}^5$	0	0.5	5.269	0.296	1.78E+08	2352.98	--
10	$3d_{3/2}^2\ 3d_{5/2}^4\ 4f_{5/2}$	1	3.5	$3d_{3/2}^3\ 3d_{5/2}^4$	0	2.5	8.661	0.446	1.81E+08	1431.52	1431.57
10	$3d_{3/2}^2\ 3d_{5/2}^4\ 4f_{5/2}$	1	2.5	$3d_{3/2}^3\ 3d_{5/2}^4$	0	1.5	8.672	0.602	3.27E+08	1429.62	1429.96
11	$3d_{3/2}^3\ 3d_{5/2}^3\ 4f_{5/2}$	1	0.5	$3d_{3/2}^2\ 3d_{5/2}^5$	0	0.5	10.586	0.063	1.53E+08	1171.12	1171.08
11	$3d_{3/2}^3\ 3d_{5/2}^3\ 4f_{5/2}$	1	0.5	$3d_{3/2}^2\ 3d_{5/2}^5$	0	0.5	10.547	0.041	9.99E+07	1175.47	1175.83
12	$3d_{3/2}^2\ 3d_{5/2}^4\ ^4p_{1/2}$	1	1.5	$3d_{3/2}^3\ 3d_{5/2}^4$	0	2.5	8.881	0.117	1.00E+08	1396.04	1396.62
12	$3d_{3/2}^2\ 3d_{5/2}^4\ 4p_{1/2}$	1	2.5	$3d_{3/2}^3\ 3d_{5/2}^4$	0	3.5	8.866	0.179	1.02E+08	1398.31	1397.57
13	$3d_{3/2}^3\ 3d_{5/2}^3\ 4p_{1/2}$	1	1.5	$3d_{3/2}^2\ 3d_{5/2}^5$	0	0.5	5.211	0.386	1.14E+08	2379.16	--
14	$3d_{3/2}^2\ 3d_{5/2}^4\ 4f_{5/2}$	1	6.5	$3d_{3/2}^3\ 3d_{5/2}^4$	0	5.5	14.667	0.148	9.87E+07	845.30	--

Table 2. Strong electric dipole transitions atomic data calculated for n=3- 4 of the iron ions Fe II–Fe V

peak #	configuration (up)	P (up)	J (up)	configuration (low)	P (low)	J (low)	ΔE (eV)	gfij	Ar (s^{-1})	λ (Å)	λ_{NIST}(Å)
Fe III											
1	$3d_{3/2}^2\ 3d_{5/2}^3\ 4f_{7/2}$	1	4	$3d_{3/2}^2\ 3d_{5/2}^4$	0	4	2.07E+01	0.786	1.62E+09	599.18	598.53
1	$3d_{3/2}^3\ 3d_{5/2}^2\ 4f_{7/2}$	1	0	$3d_{3/2}^3\ 3d_{5/2}^3$	0	1	2.07E+01	0.095	1.77E+09	599.18	598.53
1	$3d_{3/2}^2\ 3d_{5/2}^3\ 4f_{7/2}$	1	2	$3d_{3/2}^2\ 3d_{5/2}^4$	0	2	2.07E+01	0.312	1.16E+09	598.58	598.53
1	$3d_{5/2}^5\ 4f_{5/2}$	1	3	$3d_{3/2}\ 3d_{5/2}^5$	0	3	2.07E+01	0.395	1.05E+09	598.92	598.53
1	$3d_{5/2}^5\ 4f_{5/2}$	1	2	$3d_{3/2}^3\ 3d_{5/2}^3$	0	1	2.07E+01	0.207	7.71E+08	598.57	598.53
1	$3d_{3/2}\ 3d_{5/2}^4\ 4f_{5/2}$	1	5	$3d_{3/2}^2\ 3d_{5/2}^4$	0	4	2.07E+01	1.123	1.90E+09	598.43	598.53
1	$3d_{3/2}^2\ 3d_{5/2}^3\ 4f_{5/2}$	1	4	$3d_{3/2}\ 3d_{5/2}^5$	0	3	2.07E+01	0.898	1.86E+09	598.41	598.53
2	$3d_{3/2}^2\ 3d_{5/2}^3\ 4f_{7/2}$	1	6	$3d_{3/2}^3\ 3d_{5/2}^3$	0	6	2.24E+01	0.766	1.29E+09	553.04	--
2	$3d_{3/2}^2\ 3d_{5/2}^3\ 4f_{7/2}$	1	5	$3d_{3/2}^2\ 3d_{5/2}^3\ 4s_{1/2}$	0	5	2.24E+01	0.590	1.17E+09	553.86	--
2	$3d_{3/2}^2\ 3d_{5/2}^3\ 4f_{7/2}$	1	6	$3d_{3/2}^2\ 3d_{5/2}^3\ 4s_{1/2}$	0	5	2.24E+01	1.369	2.29E+09	553.68	--
3	$3d_{3/2}\ 3d_{5/2}^4\ 4f_{7/2}$	1	5	$3d_{3/2}^2\ 3d_{5/2}^4$	0	4	2.27E+01	0.702	1.42E+09	546.94	--
3	$3d_{3/2}^2\ 3d_{5/2}^3\ 4f_{5/2}$	1	5	$3d_{3/2}^2\ 3d_{5/2}^4$	0	4	2.27E+01	0.382	7.74E+08	546.89	--
4	$3d_{3/2}\ 3d_{5/2}^4\ 4f_{7/2}$	1	7	$3d_{3/2}^3\ 3d_{5/2}^3$	0	6	2.56E+01	0.391	7.40E+08	484.53	--
4	$3d_{3/2}^2\ 3d_{5/2}^3\ 4f_{7/2}$	1	3	$3d_{3/2}^2\ 3d_{5/2}^4$	0	2	2.56E+01	0.164	6.66E+08	484.58	--
5	$3d_{3/2}^2\ 3d_{5/2}^3\ 4p_{1/2}$	1	3	$3d_{3/2}^2\ 3d_{5/2}^4$	0	4	1.20E+01	1.064	7.38E+08	1033.49	1033.82
6	$3d_{3/2}^2\ 3d_{5/2}^3\ 4f_{5/2}$	1	4	$3d_{3/2}^2\ 3d_{5/2}^4$	0	4	2.52E+01	0.329	1.00E+09	492.59	--
6	$3d_{3/2}^2\ 3d_{5/2}^3\ 4f_{7/2}$	1	2	$3d_{3/2}\ 3d_{5/2}^5$	0	3	2.52E+01	0.152	8.33E+08	492.75	--
6	$3d_{3/2}\ 3d_{5/2}^4\ 4f_{5/2}$	1	3	$3d_{3/2}^2\ 3d_{5/2}^4$	0	4	2.52E+01	0.158	6.19E+08	492.45	--
6	$3d_{3/2}\ 3d_{5/2}^4\ 4f_{7/2}$	1	2	$3d_{3/2}\ 3d_{5/2}^5$	0	3	2.52E+01	0.207	1.14E+09	492.65	--
6	$3d_{3/2}\ 3d_{5/2}^4\ 4f_{7/2}$	1	3	$3d_{3/2}^2\ 3d_{5/2}^4$	0	4	2.52E+01	0.174	6.87E+08	492.05	--
7	$3d_{3/2}^2\ 3d_{5/2}^3\ 4p_{1/2}$	1	2	$3d_{3/2}^2\ 3d_{5/2}^4$	0	4	1.23E+01	0.806	7.60E+08	1005.13	1005.1
8	$3d_{3/2}^2\ 3d_{5/2}^3\ 4p_{1/2}$	1	4	$3d_{3/2}^2\ 3d_{5/2}^4$	0	2	1.18E+01	0.314	6.31E+08	1051.53	1052.75
9	$3d_{3/2}^2\ 3d_{5/2}^3\ 4p_{1/2}$	1	2	$3d_{3/2}\ 3d_{5/2}^5$	0	3	1.33E+01	0.410	6.30E+08	932.17	932.68
10	$3d_{3/2}^2\ 3d_{5/2}^3\ 4f_{5/2}$	1	5	$3d_{3/2}^2\ 3d_{5/2}^4$	0	4	2.41E+01	0.299	6.84E+08	514.79	--
10	$3d_{3/2}^2\ 3d_{5/2}^3\ 4f_{7/2}$	1	4	$3d_{3/2}^2\ 3d_{5/2}^4$	0	4	2.41E+01	0.478	1.34E+09	514.07	--
11	$3d_{5/2}\ 4f_{7/2}$	1	3	$3d_{3/2}^2\ 3d_{5/2}^4$	0	2	2.46E+01	0.185	6.95E+08	503.24	--
11	$3d_{5/2}\ 4f_{7/2}$	1	2	$3d_{3/2}^2\ 3d_{5/2}^4$	0	2	2.46E+01	0.141	7.43E+08	503.19	--
12	$3d_{3/2}^2\ 3d_{5/2}^3\ 4p_{1/2}$	1	3	$3d_{3/2}^2\ 3d_{5/2}^4$	0	4	1.57E+01	0.434	6.67E+08	787.54	787.66
13	$3d_{3/2}^2\ 3d_{5/2}^3\ 4p_{1/2}$	1	3	$3d_{3/2}^2\ 3d_{5/2}^4$	0	4	1.40E+01	0.672	8.17E+08	885.00	885.20
14	$3d_{3/2}^2\ 3d_{5/2}^3\ 4f_{7/2}$	1	5	$3d_{3/2}^2\ 3d_{5/2}^3\ 4s_{1/2}$	0	5	2.17E+01	0.494	9.16E+08	571.83	--
14	$3d_{3/2}^2\ 3d_{5/2}^3\ 4f_{7/2}$	1	6	$3d_{3/2}^2\ 3d_{5/2}^3\ 4s_{1/2}$	0	5	2.17E+01	0.529	8.30E+08	571.77	--
14	$3d_{3/2}^2\ 3d_{5/2}^3\ 4f_{5/2}$	1	2	$3d_{3/2}^3\ 3d_{5/2}^3$	0	1	2.17E+01	0.182	7.47E+08	570.81	--
14	$3d_{3/2}\ 3d_{5/2}^4\ 4f_{7/2}$	1	3	$3d_{3/2}^2\ 3d_{5/2}^4$	0	2	2.17E+01	0.216	6.33E+08	570.84	--
14	$3d_{3/2}\ 3d_{5/2}^4\ 4f_{5/2}$	1	4	$3d_{3/2}\ 3d_{5/2}^5$	0	3	2.17E+01	0.610	1.39E+09	570.65	--

Table 2. Strong electric dipole transitions atomic data calculated for n=3- 4 of the iron ions Fe II–Fe V

peak #	configuration (up)	P (up)	J (up)	configuration (low)	P (low)	J (low)	ΔE (eV)	gfij	Ar (s^{-1})	λ (Å)	λ_{NIST}(Å)
Fe IV											
1	$3d_{3/2}^2\ 3d_{5/2}^2\ 4f_{5/2}$	1	5.5	$3d_{3/2}^2\ 3d_{5/2}^3$	0	4.5	3.55E+01	1.164	5.30E+09	349.30	--
1	$3d_{3/2}\ 3d_{5/2}^3\ 4f_{5/2}$	1	6.5	$3d_{3/2}^2\ 3d_{5/2}^3$	0	5.5	3.56E+01	1.547	6.06E+09	348.68	--
1	$3d_{3/2}^2\ 3d_{5/2}^2\ 4f_{5/2}$	1	2.5	$3d_{3/2}\ 3d_{5/2}^4$	0	3.5	3.55E+01	0.227	2.07E+09	348.81	--
1	$3d_{3/2}\ 3d_{5/2}^3\ 4f_{5/2}$	1	3.5	$3d_{3/2}^2\ 3d_{5/2}^3$	0	4.5	3.56E+01	0.301	2.07E+09	348.46	--
1	$3d_{3/2}^2\ 3d_{5/2}^2\ 4f_{5/2}$	1	5.5	$3d_{3/2}^2\ 3d_{5/2}^3$	0	4.5	3.56E+01	0.961	4.40E+09	348.45	--
1	$3d_{3/2}^3\ 3d_{5/2}\ 4f_{5/2}$	1	6.5	$3d_{3/2}\ 3d_{5/2}^4$	0	5.5	3.56E+01	1.140	4.47E+09	348.59	--
2	$3d_{3/2}^2\ 3d_{5/2}^2\ 4f_{5/2}$	1	5.5	$3d_{3/2}^2\ 3d_{5/2}^3$	0	5.5	3.66E+01	0.489	2.37E+09	338.68	--
2	$3d_{3/2}^2\ 3d_{5/2}^2\ 4f_{7/2}$	1	6.5	$3d_{3/2}^2\ 3d_{5/2}^3$	0	5.5	3.66E+01	1.557	6.47E+09	338.65	--
2	$3d_{3/2}^2\ 3d_{5/2}^2\ 4f_{7/2}$	1	5.5	$3d_{3/2}^2\ 3d_{5/2}^3$	0	5.5	3.66E+01	0.350	1.70E+09	338.40	--
2	$3d_{3/2}^2\ 3d_{5/2}^2\ 4f_{5/2}$	1	7.5	$3d_{3/2}^2\ 3d_{5/2}^3$	0	6.5	3.67E+01	1.835	6.69E+09	338.07	--
2	$3d_{3/2}^2\ 3d_{5/2}^2\ 4f_{7/2}$	1	4.5	$3d_{3/2}^2\ 3d_{5/2}^3$	0	4.5	3.67E+01	0.373	2.18E+09	338.08	--
2	$3d_{3/2}^2\ 3d_{5/2}^2\ 4f_{7/2}$	1	5.5	$3d_{3/2}\ 3d_{5/2}^4$	0	5.5	3.66E+01	0.511	2.48E+09	338.43	--
3	$3d_{3/2}^3\ 3d_{5/2}\ 4f_{7/2}$	1	1.5	$3d_{5/2}$	0	2.5	3.62E+01	0.130	1.85E+09	342.52	--
3	$3d_{3/2}^2\ 3d_{5/2}^2\ 4f_{7/2}$	1	0.5	$3d_{3/2}^2\ 3d_{5/2}^3$	0	1.5	3.62E+01	0.070	1.99E+09	342.78	--
3	$3d_{3/2}^3\ 3d_{5/2}\ 4f_{7/2}$	1	3.5	$3d_{3/2}^2\ 3d_{5/2}^3$	0	3.5	3.61E+01	0.295	2.09E+09	342.98	--
3	$3d_{3/2}^2\ 3d_{5/2}^2\ 4f_{7/2}$	1	4.5	$3d_{3/2}^2\ 3d_{5/2}^3$	0	4.5	3.62E+01	0.341	1.94E+09	342.16	--
4	$3d_{3/2}^3\ 3d_{5/2}\ 4f_{5/2}$	1	3.5	$3d_{3/2}^2\ 3d_{5/2}^3$	0	2.5	3.84E+01	0.380	3.04E+09	322.65	--
4	$3d_{3/2}^2\ 3d_{5/2}^2\ 4f_{5/2}$	1	4.5	$3d_{3/2}^2\ 3d_{5/2}^3$	0	3.5	3.85E+01	0.517	3.31E+09	322.43	--
4	$3d_{3/2}^2\ 3d_{5/2}^2\ 4f_{7/2}$	1	5.5	$3d_{3/2}^2\ 3d_{5/2}^3$	0	4.5	3.85E+01	0.630	3.37E+09	322.20	--
4	$3d_{3/2}\ 3d_{5/2}^3\ 4f_{7/2}$	1	6.5	$3d_{3/2}^2\ 3d_{5/2}^3$	0	5.5	3.85E+01	0.772	3.55E+09	321.94	--
4	$3d_{3/2}^3\ 3d_{5/2}\ 4f_{5/2}$	1	2.5	$3d_{3/2}^2\ 3d_{5/2}^3$	0	2.5	3.85E+01	0.456	4.89E+09	321.96	--
4	$3d_{3/2}^2\ 3d_{5/2}^2\ 4f_{7/2}$	1	4.5	$3d_{3/2}^2\ 3d_{5/2}^3$	0	3.5	3.85E+01	0.390	2.51E+09	321.95	--
5	$3d_{3/2}\ 3d_{5/2}^3\ 4f_{5/2}$	1	3.5	$3d_{3/2}^2\ 3d_{5/2}^3$	0	2.5	3.93E+01	0.473	3.97E+09	315.44	--
5	$3d_{3/2}^2\ 3d_{5/2}^2\ 4f_{7/2}$	1	4.5	$3d_{3/2}^2\ 3d_{5/2}^3$	0	3.5	3.93E+01	0.460	3.08E+09	315.30	--
5	$3d_{3/2}\ 3d_{5/2}^3\ 4f_{5/2}$	1	2.5	$3d_{3/2}^2\ 3d_{5/2}^3$	0	2.5	3.93E+01	0.242	2.71E+09	315.34	--
5	$3d_{3/2}^2\ 3d_{5/2}^2\ 4f_{7/2}$	1	5.5	$3d_{3/2}^2\ 3d_{5/2}^3$	0	4.5	3.93E+01	0.499	2.79E+09	315.09	--
5	$3d_{3/2}^2\ 3d_{5/2}^2\ 4f_{5/2}$	1	3.5	$3d_{3/2}^2\ 3d_{5/2}^3$	0	3.5	3.93E+01	0.332	2.78E+09	315.12	--
5	$3d_{3/2}\ 3d_{5/2}^3\ 4f_{7/2}$	1	4.5	$3d_{3/2}^2\ 3d_{5/2}^3$	0	3.5	3.93E+01	0.394	2.64E+09	315.11	--
5	$3d_{3/2}\ 3d_{5/2}^3\ 4f_{5/2}$	1	3.5	$3d_{3/2}\ 3d_{5/2}^4$	0	2.5	3.93E+01	0.249	2.09E+09	315.33	--
5	$3d_{3/2}\ 3d_{5/2}^3\ 4f_{5/2}$	1	2.5	$3d_{3/2}\ 3d_{5/2}^4$	0	1.5	3.93E+01	0.174	1.95E+09	315.21	--
5	$3d_{5/2}^4\ 4f_{5/2}$	1	1.5	$3d_{3/2}^2\ 3d_{5/2}^3$	0	0.5	3.94E+01	0.130	2.18E+09	315.03	--
6	$3d_{3/2}^2\ 3d_{5/2}^2\ 4f_{5/2}$	1	3.5	$3d_{3/2}\ 3d_{5/2}^4$	0	2.5	3.48E+01	0.579	3.81E+09	355.95	--
6	$3d_{3/2}^3\ 3d_{5/2}\ 4f_{7/2}$	1	2.5	$3d_{3/2}^2\ 3d_{5/2}^3$	0	1.5	3.49E+01	0.234	2.05E+09	355.73	--
6	$3d_{3/2}^2\ 3d_{5/2}^2\ 4f_{7/2}$	1	0.5	$3d_{3/2}^2\ 3d_{5/2}^3$	0	0.5	3.49E+01	0.090	2.39E+09	355.52	--
6	$3d_{3/2}\ 3d_{5/2}^3\ 4f_{5/2}$	1	4.5	$3d_{3/2}^2\ 3d_{5/2}^3$	0	3.5	3.48E+01	0.638	3.35E+09	356.70	--
8	$3d_{3/2}\ 3d_{5/2}^3\ 4f_{7/2}\ 3$	1	6.5	$3d_{3/2}\ 3d_{5/2}^4$	0	5.5	4.14E+01	0.407	2.17E+09	299.35	--
9	$3d_{3/2}^3\ 3d_{5/2}\ 4p_{1/2}$	1	5.5	$3d_{3/2}^2\ 3d_{5/2}^3$	0	5.5	2.18E+01	1.100	1.90E+09	567.42	--
10	$3d_{3/2}\ 3d_{5/2}^3\ 4f_{7/2}$	1	2.5	$3d_{3/2}^2\ 3d_{5/2}^3$	0	2.5	3.42E+01	0.317	2.68E+09	362.02	--
11	$3d_{3/2}\ 3d_{5/2}^3\ 4f_{7/2}$	1	3.5	$3d_{3/2}^2\ 3d_{5/2}^3$	0	2.5	3.27E+01	0.325	1.88E+09	379.69	--
11	$3d_{3/2}\ 3d_{5/2}^3\ 4f_{7/2}$	1	3.5	$3d_{3/2}\ 3d_{5/2}^4$	0	3.5	3.26E+01	0.352	2.03E+09	379.92	--
11	$3d_{3/2}\ 3d_{5/2}^3\ 4f_{7/2}$	1	4.5	$3d_{3/2}^2\ 3d_{5/2}^3$	0	4.5	3.27E+01	0.361	1.67E+09	379.42	--
11	$3d_{3/2}\ 3d_{5/2}^3\ 4f_{7/2}$	1	4.5	$3d_{3/2}\ 3d_{5/2}^4$	0	3.5	3.27E+01	0.734	3.40E+09	379.62	--
11	$3d_{3/2}\ 3d_{5/2}^3\ 4f_{7/2}$	1	0.5	$3d_{3/2}^2\ 3d_{5/2}^3$	0	0.5	3.26E+01	0.071	1.64E+09	380.07	--

Table 2. Strong electric dipole transitions atomic data calculated for n=3- 4 of the iron ions Fe II–Fe V

peak #	configuration (up)	P (up)	J (up)	configuration (low)	P (low)	J (low)	ΔE (eV)	gfij	Ar (s^{-1})	λ (Å)	λ_{NIST}(Å)
Fe V											
1	$3d_{3/2}^2\ 3d_{5/2}\ 4f_{7/2}$	1	1	$3d_{3/2}^2\ 3d_{5/2}^2$	0	0	5.25E+01	0.164	6.55E+09	236.14	--
1	$3d_{3/2}\ 3d_{5/2}^2\ 4f_{5/2}$	1	2	$3d_{3/2}^3\ 3d_{5/2}$	0	1	5.25E+01	0.339	8.13E+09	236.02	--
1	$3d_{3/2}\ 3d_{5/2}^2\ 4f_{5/2}$	1	2	$3d_{3/2}^2\ 3d_{5/2}^2$	0	2	5.25E+01	0.219	5.23E+09	236.14	--
1	$3d_{3/2}^3\ 4f_{5/2}$	1	1	$3d_{3/2}^3\ 3d_{5/2}$	0	1	5.25E+01	0.137	5.45E+09	236.13	--
1	$3d_{3/2}\ 3d_{5/2}^2\ 4f_{5/2}$	1	2	$3d_{3/2}^3\ 3d_{5/2}$	0	1	5.25E+01	0.656	1.57E+10	236.03	--
1	$3d_{3/2}\ 3d_{5/2}^2\ 4f_{5/2}$	1	2	$3d_{5/2}^4$	0	2	5.25E+01	0.344	8.24E+09	236.00	--
1	$3d_{3/2}\ 3d_{5/2}^2\ 4f_{7/2}$	1	5	$3d_{3/2}\ 3d_{5/2}^3$	0	4	5.25E+01	1.178	1.28E+10	236.11	--
2	$3d_{3/2}^2\ 3d_{5/2}\ 4f_{7/2}$	1	4	$3d_{3/2}^3\ 3d_{5/2}$	0	3	5.14E+01	0.360	4.58E+09	241.22	--
2	$3d_{3/2}^2\ 3d_{5/2}\ 4f_{7/2}$	1	5	$3d_{3/2}^2\ 3d_{5/2}^2$	0	4	5.14E+01	0.409	4.26E+09	241.25	--
2	$3d_{3/2}\ 3d_{5/2}^2\ 4f_{5/2}$	1	5	$3d_{3/2}\ 3d_{5/2}^3$	0	4	5.14E+01	2.591	2.70E+10	241.35	--
2	$3d_{3/2}\ 3d_{5/2}^2\ 4f_{5/2}$	1	3	$3d_{3/2}^3\ 3d_{5/2}$	0	3	5.13E+01	0.283	4.62E+09	241.75	--
2	$3d_{3/2}\ 3d_{5/2}^2\ 4f_{5/2}$	1	3	$3d_{3/2}\ 3d_{5/2}^3$	0	2	5.13E+01	0.710	1.16E+10	241.87	--
2	$3d_{5/2}^3\ 4f_{5/2}$	1	2	$3d_{3/2}\ 3d_{5/2}^3$	0	2	5.13E+01	0.264	6.02E+09	241.75	--
2	$3d_{5/2}^3\ 4f_{5/2}$	1	2	$3d_{3/2}\ 3d_{5/2}^3$	0	1	5.13E+01	0.546	1.25E+10	241.79	--
2	$3d_{3/2}\ 3d_{5/2}^2\ 4f_{7/2}$	1	4	$3d_{3/2}\ 3d_{5/2}^3$	0	3	5.14E+01	0.876	1.11E+10	241.25	--
3	$3d_{3/2}\ 3d_{5/2}^2\ 4f_{7/2}$	1	0	$3d_{3/2}\ 3d_{5/2}^3$	0	1	4.99E+01	0.131	1.42E+10	248.55	--
3	$3d_{3/2}^3\ 4f_{5/2}$	1	3	$3d_{5/2}^4$	0	2	4.98E+01	0.355	5.45E+09	248.97	--
3	$3d_{5/2}^3\ 4f_{5/2}$	1	3	$3d_{3/2}^2\ 3d_{5/2}^2$	0	2	4.99E+01	0.617	9.52E+09	248.59	--
3	$3d_{3/2}\ 3d_{5/2}^2\ 4f_{5/2}$	1	1	$3d_{5/2}^4$	0	0	4.99E+01	0.148	5.32E+09	248.59	--
4	$3d_{5/2}^3\ 4p_{1/2}$	1	2	$3d_{3/2}\ 3d_{5/2}^3$	0	3	2.89E+01	1.065	7.74E+09	428.31	--
5	$3d_{3/2}\ 3d_{5/2}^2\ 4f_{7/2}$	1	5	$3d_{3/2}^2\ 3d_{5/2}^2$	0	4	4.73E+01	0.458	4.05E+09	261.84	--
5	$3d_{3/2}\ 3d_{5/2}^2\ 4f_{7/2}$	1	3	$3d_{3/2}\ 3d_{5/2}^3$	0	3	4.74E+01	0.427	5.95E+09	261.38	--
6	$3d_{3/2}^2\ 3d_{5/2}\ 4f_{7/2}$	1	2	$3d_{3/2}^3\ 3d_{5/2}$	0	1	4.88E+01	0.208	4.31E+09	254.02	--
6	$3d_{3/2}\ 3d_{5/2}^2\ 4f_{7/2}$	1	4	$3d_{3/2}\ 3d_{5/2}^3$	0	4	4.88E+01	0.690	7.90E+09	254.30	--
6	$3d_{3/2}\ 3d_{5/2}^2\ 4f_{7/2}$	1	5	$3d_{3/2}^2\ 3d_{5/2}^2$	0	5	4.88E+01	0.870	8.17E+09	254.11	--
7	$3d_{3/2}\ 3d_{5/2}^2\ 4p_{1/2}$	1	3	$3d_{3/2}\ 3d_{5/2}^3$	0	4	3.34E+01	0.631	4.35E+09	371.69	--
7	$3d_{3/2}\ 3d_{5/2}^2\ 4f_{7/2}$	1	3	$3d_{3/2}^2\ 3d_{5/2}^2$	0	2	4.54E+01	0.585	7.49E+09	272.84	--
7	$3d_{3/2}\ 3d_{5/2}^2\ 4f_{5/2}$	1	2	$3d_{3/2}^2\ 3d_{5/2}^2$	0	2	4.55E+01	0.583	1.05E+10	272.34	--
8	$3d_{3/2}^2\ 3d_{5/2}\ 4f_{7/2}$	1	5	$3d_{3/2}^2\ 3d_{5/2}^2$	0	4	5.34E+01	1.851	2.08E+10	232.38	--
8	$3d_{3/2}\ 3d_{5/2}^2\ 4f_{7/2}$	1	4	$3d_{3/2}\ 3d_{5/2}^3$	0	3	5.34E+01	1.463	2.01E+10	232.38	--
8	$3d_{3/2}\ 3d_{5/2}^2\ 4f_{5/2}$	1	3	$3d_{3/2}^2\ 3d_{5/2}^2$	0	2	5.34E+01	1.125	1.99E+10	232.28	--
9	$3d_{3/2}^2\ 3d_{5/2}\ 4f_{5/2}$	1	2	$3d_{3/2}^2\ 3d_{5/2}^2$	0	2	5.50E+01	0.228	5.98E+09	225.54	--
9	$3d_{3/2}^2\ 3d_{5/2}\ 4f_{5/2}$	1	3	$3d_{3/2}^2\ 3d_{5/2}^2$	0	2	5.50E+01	0.606	1.14E+10	225.52	--
9	$3d_{3/2}^2\ 3d_{5/2}\ 4f_{7/2}$	1	4	$3d_{3/2}^2\ 3d_{5/2}^2$	0	3	5.49E+01	0.915	1.33E+10	225.69	--
10	$3d_{3/2}^3\ 4p_{1/2}$	1	0	$3d_{3/2}^3\ 3d_{5/2}$	0	1	3.11E+01	0.164	6.92E+09	398.12	398.08
10	$3d_{3/2}^2\ 3d_{5/2}\ 4p_{1/2}$	1	1	$3d_{3/2}^2\ 3d_{5/2}^2$	0	2	3.11E+01	0.271	3.81E+09	398.12	398.38
10	$3d_{3/2}\ 3d_{5/2}^2\ 4p_{1/2}$	1	4	$3d_{3/2}\ 3d_{5/2}^3$	0	4	3.11E+01	0.877	4.09E+09	398.68	398.42
11	$3d_{3/2}\ 3d_{5/2}^2\ 4p_{1/2}$	1	5	$3d_{3/2}^2\ 3d_{5/2}^2$	0	6	3.05E+01	2.638	9.65E+09	407.15	407.41